

Timing

Andrea Grossutti, mat. 1237344
Alessandro Lovo, mat. 1236048
Leonardo Zampieri, mat. 1237351

December 3, 2019

1 Aims

- Energy calibration of the organic scintillators and calculation of the energy resolution from the analysis of the Compton edge;
- Optimization of the external delay of the analog CFTD to obtain the best time resolution;
- Study of the time resolution behavior as a function of the energy;
- Comparison between the timing resolutions obtained from analog and digital treatment of the signals;
- Measurement of the speed of light.

2 Experimental setup

The experimental setup consists of two collinear organic scintillators (DET 1 and DET 2), mounted on a sledge and facing each other. Between them there is a ^{22}Na source collimated by two lead bricks. The energy peaks of photons emitted by this source are shown in Table 1.

Photopeak [keV]	Compton edge [keV]
511.0	340.7
1274.537	1061.7

Table 1: Gamma radiation for ^{22}Na from NuDat, <https://www.nndc.bnl.gov/nudat2/decaysearchdirect.jsp?nuc=22NA&unc=nds>

Data are collected from the detectors through a electronic chain: a fan-in-fan-out quad module replicates the signal of each detector and produces four copies of it; then, through a Constant Fraction Time Discriminator (CFTD), a logic signal is produced. The CFTD trigger threshold has been set so that the noise is discarded, while the interesting signals produce an output. From the CFTD the logic signal runs through a coincidence unit, used as a trigger. Besides, the logic signal of DET 1 runs into the *start* of a Time to Amplitude Converter (TAC) module, while the one from DET 2 passes through a delay module and then runs into the *stop* of the TAC. A digitizer, triggered by the coincidence unit, acquires the energy spectra of both detectors and the time spectrum of the TAC.

3 Apparatus calibration

3.1 Calibration of detectors

Disabling the coincidence unit in order to collect both peaks of the ^{22}Na source, a spectrum for each detector is acquired. Due to the chemical composition of the detector (low Z materials), photopeaks are negligible and only the Compton effect is detected.

The observed Compton edge (CE) is a convolution of the real CE with a gaussian noise with mean 0 and sigma σ_{res} due to the detector finite resolution; this convolution results in a shift of the maximum of the CE towards lower energies. So, in order to calibrate the detectors, an estimate of this shift is needed.

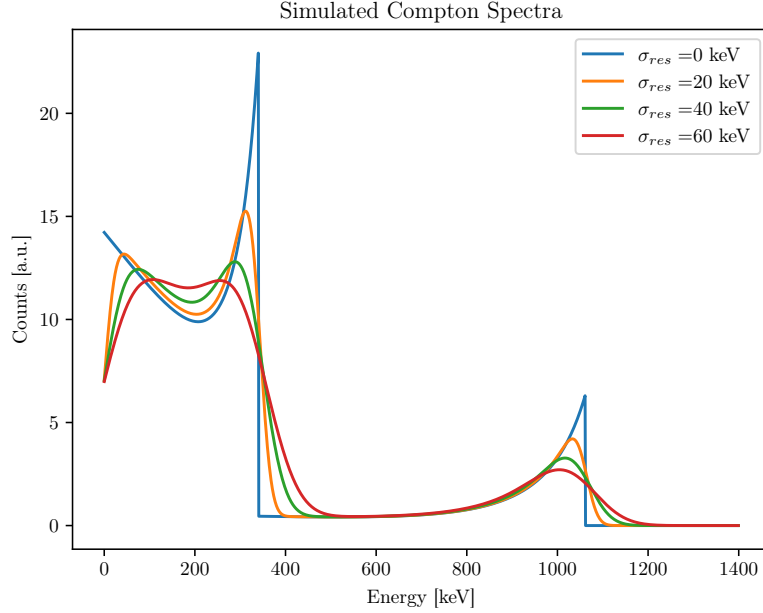


Figure 1: Simulated Compton spectra with different values of σ_{res} . Even if here the two peaks are represented together, they were analyzed independently.

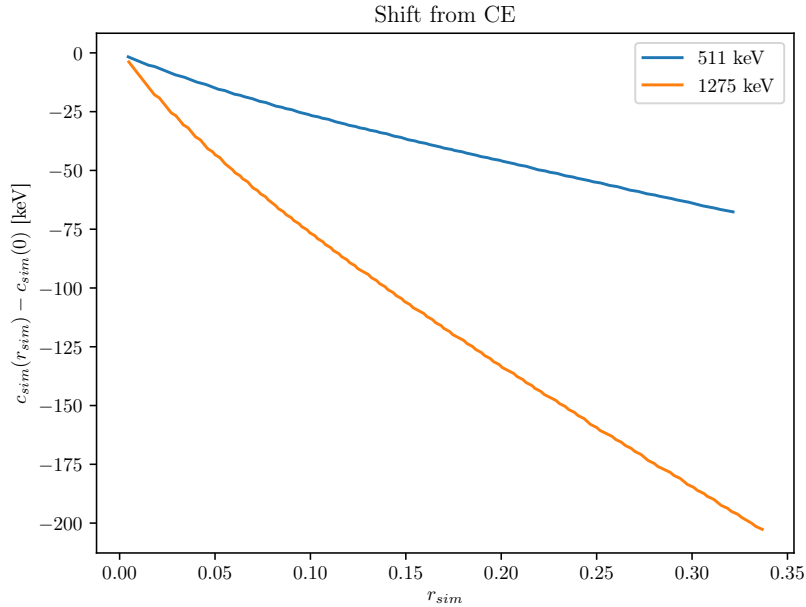


Figure 2: Relation between the resolution of the peak and the peak position, in calibrated histograms.

By simulating* the effects on CE varying σ_{res} (fig 1) the position of the peak c_{sim} and its right

*For formulas see N. Kudomi *Energy calibration of plastic scintillators for low energy electrons by using Compton scattering of γ rays*, Nuc. Instr. and Meth., 430 (1999), [https://doi.org/10.1016/S0168-9002\(99\)00200-4](https://doi.org/10.1016/S0168-9002(99)00200-4)

Half Width Half Maximum w_{sim}^\dagger can be computed, and the correlation between simulated resolution $r_{sim} = \frac{w_{sim}}{c_{sim}}$ and c_{sim} can be studied (fig 2).

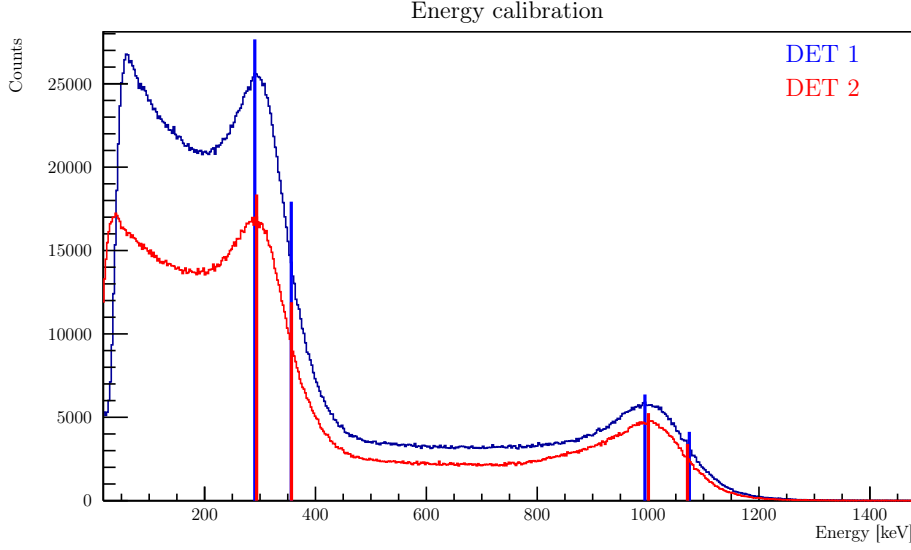


Figure 3: Position of CE's centroids and widths, in the calibrated energy spectra.

Det	p [keV]	c_{ch}	w_{ch}	c_E [keV]	w_E [keV]	r_E	σ_{res} [keV]
#1	511	3440 ± 9	736 ± 13	290.2 ± 0.7	66 ± 1	0.227 ± 0.004	38.8 ± 0.5
	1275	11312 ± 9	960 ± 13	994.1 ± 0.8	225 ± 4	0.086 ± 0.001	37.0 ± 0.5
#2	511	4400 ± 9	768 ± 13	293.8 ± 0.7	60 ± 1	0.205 ± 0.004	35.7 ± 0.6
	1275	13392 ± 9	960 ± 13	1000.5 ± 0.7	206 ± 4	0.075 ± 0.001	33.9 ± 0.5

Table 2: Centroids and widths of the CE peaks: p is the photopeak energy. The errors for the values in channels come from a uniform distribution on the bin width of the histogram. The values of c_E , w_E , r_E and σ_{res} here are the ones after the calibration process converged.

Computing c_{ch} and w_{ch} for the experimental spectra in channels (fig 3, tab 2), noting that for the peak relative to the 511 keV photon the half maximum needs to be computed with respect to the baseline due to the low energy Compton events of the 1275 keV photon, the calibration of the energy spectra can be done.

Assuming a calibration relation $E = a \cdot ch + b$, the resolution in energy is:

$$r_E = \frac{w_E}{c_E} = \frac{aw_{ch}}{ac_{ch} + b} = \frac{w_{ch}}{c_{ch} + b/a}$$

Starting from $b/a = 0$, imposing $r_E = r_{sim}$ and therefore finding c_E through the previous simulations, a calibration of the graph can be done. Updating b/a ratio with the just found values and iterating until the process converges (typically, 3-4 iterations), the results in tab 3 can be found.

[†]We used this approach instead of a gaussian fit of the peaks because both in the simulation and in the experimental spectra the result of the fit was highly dependent on the range chosen for the fit, which is arbitrary. See also Dietze, Klein: *Gamma-calibration of NE 213 scintillation counters*, Nuc. Instr. and Meth., 193 (1982), [https://doi.org/10.1016/0029-554X\(82\)90249-X](https://doi.org/10.1016/0029-554X(82)90249-X)

Det	a [keV]	b [keV]
#1	0.0894 ± 0.0002	-17 ± 2
#2	0.0786 ± 0.0002	-52 ± 2

Table 3: Calibrations coefficients after the calibration process converged.

3.2 Calibration of the TAC

By changing the delay of the delay module placed before the TAC's *stop*, we can acquire different TAC peaks and use them for calibration (fig 4). For each peak the centroid is found through gaussian fit on a small range around the maximum (tab 4).

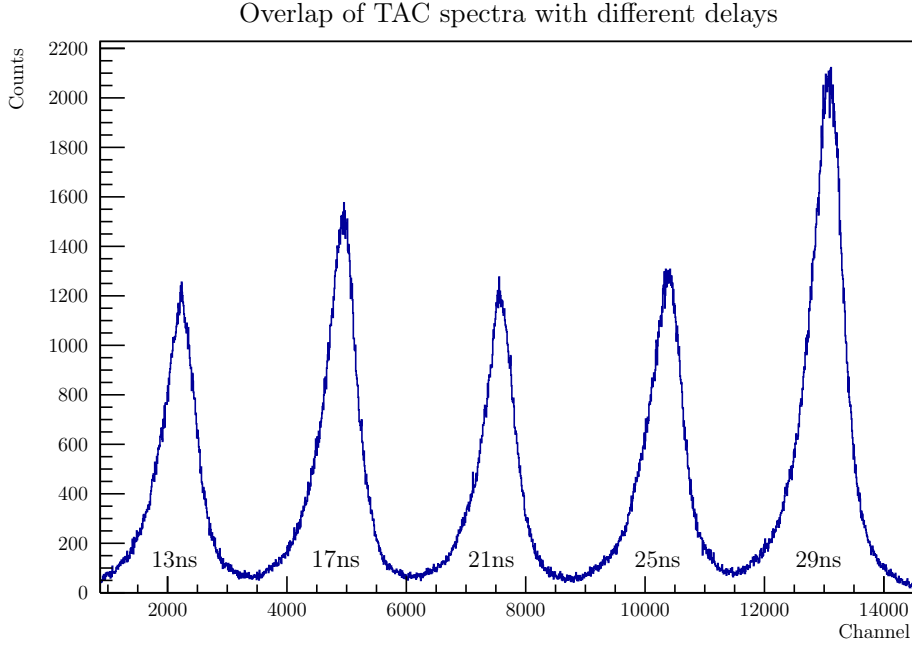


Figure 4: Different peaks with different delays. Different height of the peaks are due to different acquisition time.

Delay [ns]	Centroid [channel]
13	2235 ± 20
17	4950 ± 30
21	7555 ± 30
25	10390 ± 30
29	13080 ± 40

Table 4: TAC centroids.

The centroids are fitted using a linear relation:

$$t = m \cdot ch + q$$

$$m = (1.477 \pm 0.005)\text{ps}$$

where the q value isn't reported, having no meaning. In fact, delays are introduced in a more complex system, which already have an intrinsic delay: zero external delay therefore doesn't mean zero time in TAC.

4 LEMO calibration

A set of LEMO cables is provided. Setting external delay to 13ns and inserting one by one each LEMO cable in series with the external delay module, 5-minutes datasets are acquired; computing the difference between the observed centroids and the centroid without LEMO cable previously measured, and converting it with the calibration parameter, the time-length of each LEMO cable is computed.

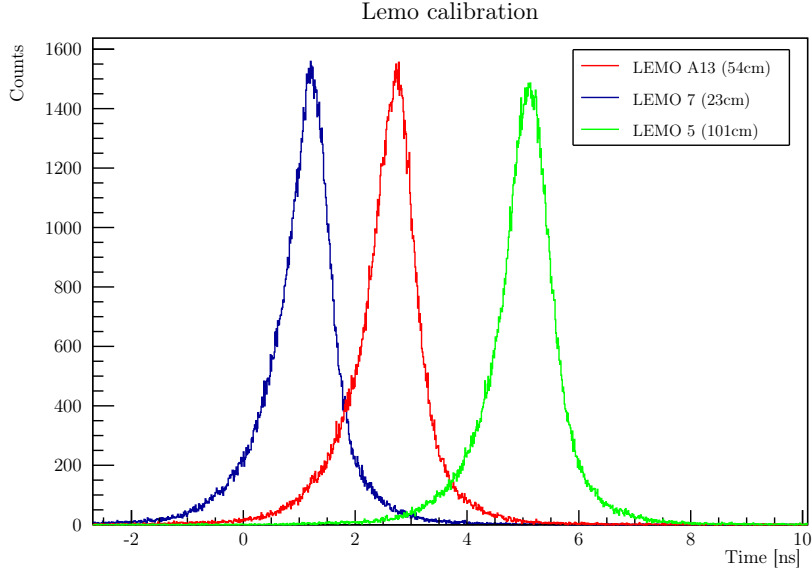


Figure 5: Some of the peaks of the LEMO cables

LEMO ID	LEMO length [cm], ± 0.1	LEMO time [ns]
6	22.5	1.17 ± 0.04
7	23.0	1.15 ± 0.04
2	53.5	2.70 ± 0.03
A13	53.5	2.71 ± 0.05
4	101.0	5.12 ± 0.04
5	101.0	5.08 ± 0.07

Table 5: LEMO cables

The time length of each LEMO cable can be compared with its metric length, finding a linear relation as expected.

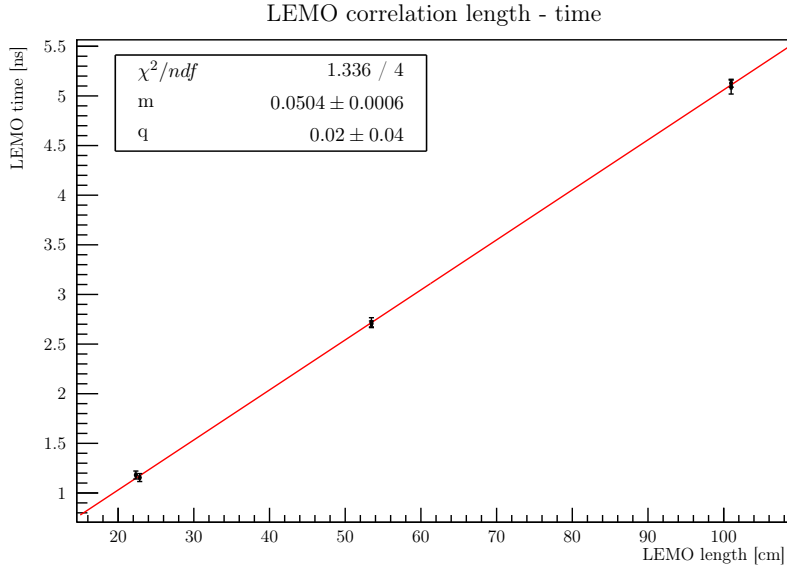


Figure 6: Relation between LEMO length and time: as expected, the dependence is confirmed.

5 CFTD delay optimization

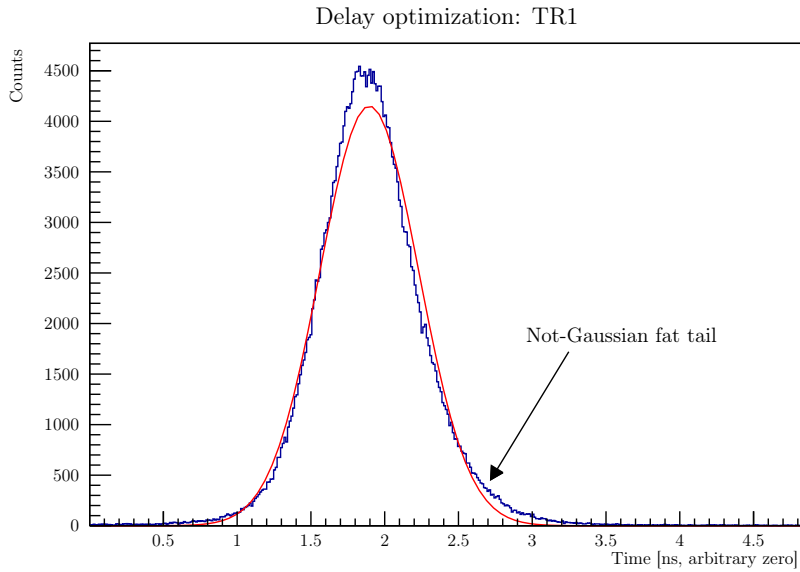


Figure 7: Initial situation: large not-gaussian shape.

The CFTD superimposes an inverted delayed copy of the signal to an attenuated one. The delay must be properly set using LEMO cables to optimize the TAC resolution. With only the default delay, the signal detected by the TAC is large and not gaussian (see fig. 7); after some tests, a setup which leads to a better resolution and a more gaussian-like output is obtained.

Different combinations of LEMO cable have been inserted in series with the pre-set delay; every time the configuration changed, the WALK ADJ potentiometer has been regulated to minimize the dispersion (see fig. 8) at the zero-crossing point of the signals.

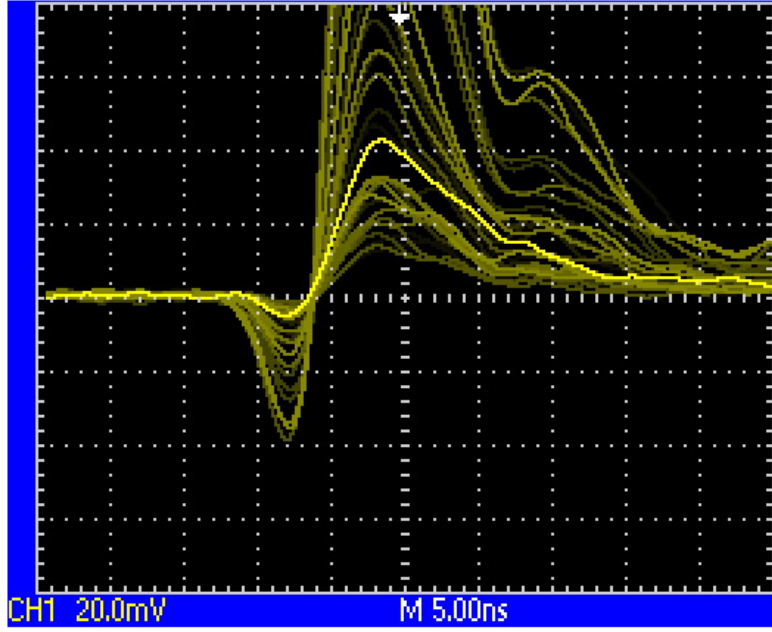


Figure 8: Monitor CFTD signal triggered on CFTD output, seen by the oscilloscope.

Fitting the obtained peaks with a gaussian and relating them to the delay inserted in the CFTDs (after some tests, we noticed that the optimal setup is with the same delay in both CFTDs), we obtain the result in fig 9. As can be seen from the figure, a minimum is found at about 3ns of delay (LEMO 13 for DET 1 and LEMO 2 for DET 2). Considering the pre-set delay (around 2ns), this lead to a optimal delay of around 5ns, that is about 80% (one minus the attenuation fraction) the rise time of the detector signal (~ 6 ns), as theoretically expected.

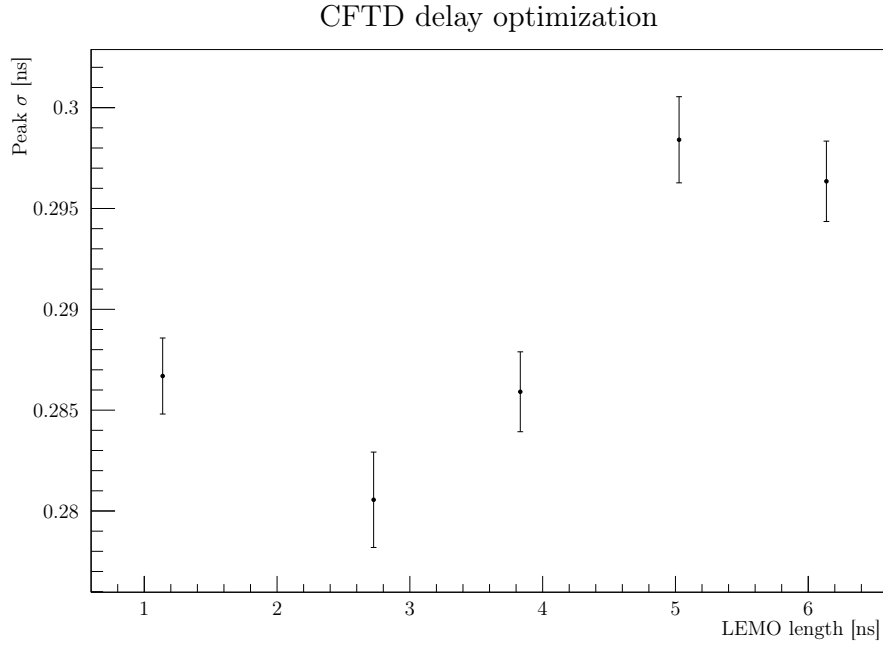


Figure 9: Optimization of the CFTD delay.

The minimum configuration has been kept for all the following measurements.

6 Time resolution as function of energy range

In order to have a wider Compton energy spectra, 20 hours of data are acquired using a ^{60}Co source. This source decays emitting two photons of energy around 1MeV: a few of them are emitted back-to-back and hence can trigger the coincidence unit (fig 10), that is set in *AND* configuration.

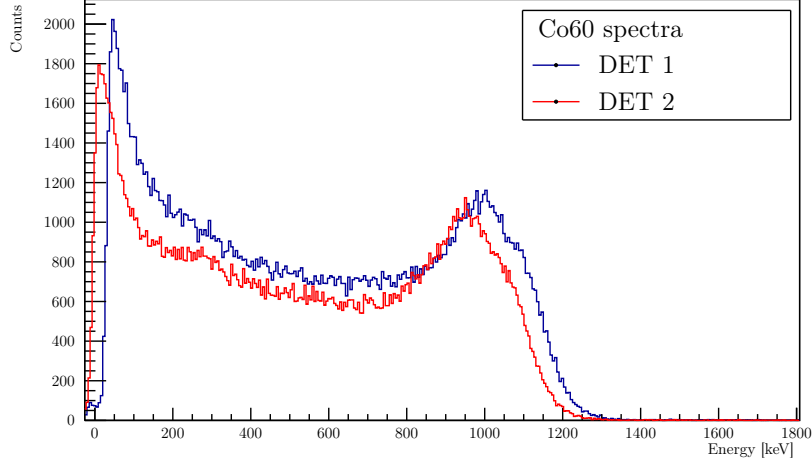


Figure 10: Energy spectra of the two detectors with ^{60}Co source. The separation between the spectra of the two detectors is due to the errors in the calibration parameters and the slight variations in high voltage supply.

Properly filtering in energy the spectra, the dependence of the resolution of the TAC can be studied. Since, despite the delay optimization, the TAC peaks still have a slightly fat-tailed distribution, the gaussian fit is not accurate. Therefore, the Full Width Half Maximum (FWHM) is used. The filtering can be done either by setting a Lower Energy Threshold (LET) or by selecting a window in energy, i.e. keeping only the data with energy between the LET and an Upper Energy Threshold (UET). The results are shown in fig 11.

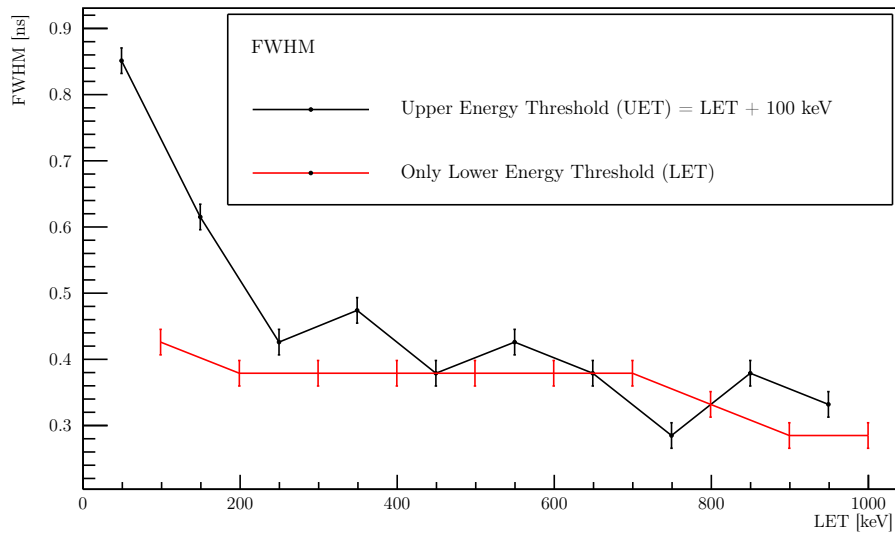


Figure 11: When computing the FWHM, the peaks had been properly rebinned in order to have them sufficiently smooth. The errors on the FWHMs come from a uniform distribution on the bin width.

From fig 11 we can see the resolution improves dramatically as we discard the events at lower energy,

and then keep to slowly improve as LET increases. An equilibrium must be found between discarding low energy events with poor time resolution and keeping enough events to have a rich statistic. This equilibrium strongly depend on the shape and the width of the source energetic spectra, and in our case it is better achieved around compton edge.

7 Speed of light

The detectors have been placed such that they're about 1.70m away. The ^{22}Na source has been placed firstly near DET 1 and then near DET 2, and the TAC signal has been acquired (one hour for each configuration); then, the centroids μ_1 and μ_2 of the two measurements have been found through a gaussian interpolation. Measuring the distance between the two source positions d , the light speed can be computed.

Observe that the two centroids have been firstly subtracted keeping them in channel and then calibrated, to prevent the introduction of correlation between the two measures.

The errors have been propagated as statistical errors. Note the high error on the distance between the positions of the source, due to the width of the source itself.

$$\begin{aligned}\mu_1 &= (16433 \pm 5)\text{channel} \\ \mu_2 &= (8966 \pm 5)\text{channel} \\ d &= (162 \pm 1)\text{cm} \\ c &= \frac{2d}{(\mu_1 - \mu_2)m} = (2.94 \pm 0.02) \cdot 10^8 \text{m s}^{-1}\end{aligned}$$

The result is compatible with the true value.

8 A-Posteriori CFTD

During the last day, again with the ^{22}Na source, we disabled the digitizer FPGA and acquired two datasets of raw waveforms directly from the detectors. This allows us to simulate an a-posteriori software CFTD and FPGA, and compare it with the analog one.

8.1 Waveforms

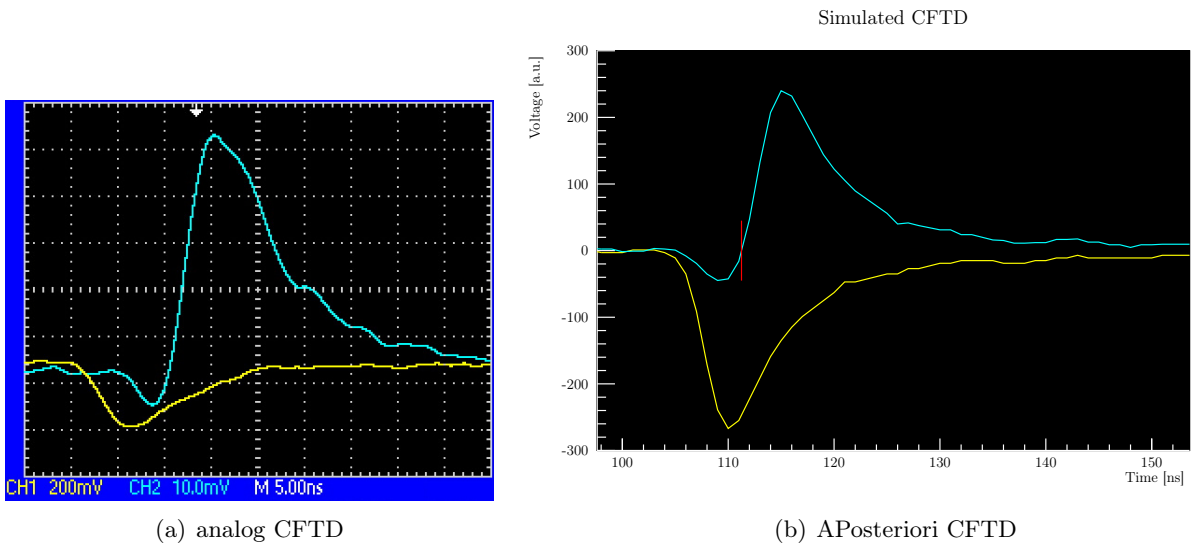


Figure 12: Waveforms (yellow) and monitor signals (cyan) for analog and software CFTD, set with the same parameters (fraction = 20%, delay $\sim 5\text{ns}$)

In fig. 12 a waveform sample is showed (yellow), as seen by oscilloscope and digitizer. The shape is, as expected, the same; in particular, both rise time (about 6ns) and falling time (about 20ns) are the same. Moreover, the signal transformed from the CFTD is also showed (cyan); it is formed by an attenuated copy of the original signal summed to a inverted delayed one. While the analog CFTD does the transformation through electronic components, the APosteriori one does it computationally. Even in this case the two systems return a similar signal; however, the shortness in time of the signal and the low time resolution of the digitizer (a sample each 1ns) result in a rougher waveform.

8.2 Energy spectra

Integrating the waveform (subtracted of the baseline) over the domain, an energy spectra can be computed. As can be seen comparing fig. 13 with fig. 3, here only the 511keV peak is visible: the trigger set on coincidences and the low acceptance of the digitized cut away the higher peak.

Even with only one peak, the comparison with the previous calibration allow us to make a rough calibration using position of peak and right half maximum (in red in figure), and using the result of the previous calibration.

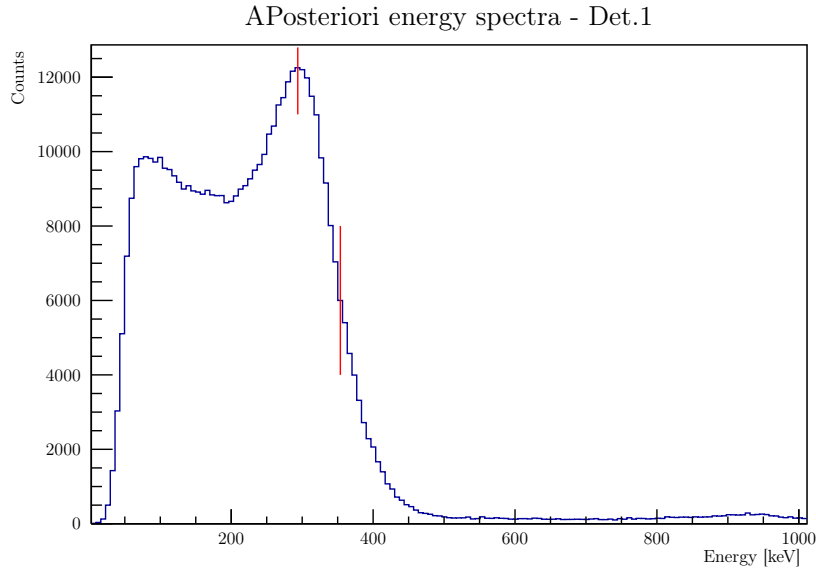


Figure 13: APosteriori energy spectra.

8.3 CFTD parameters

For each dataset, the following procedure is followed:

- Coincidences are searched, i.e. events that are recorded by both the detectors;
- For each event, a simulated CFTD is applied to the two waveforms and monitor signals are computed;
- Zero crossings are computed via a linear interpolation around the sign change;
- For each event, the time difference between the zero crossings in the two detector is computed;
- The distribution of the time difference is built and its FWHM is computed;

This procedure is repeated for different combination of CFTD delay τ (from 1 to 10ns, with 1ns step) and attenuation fraction f (from 0.1 to 0.9, with 0.1 step): the results are shown in fig 14.

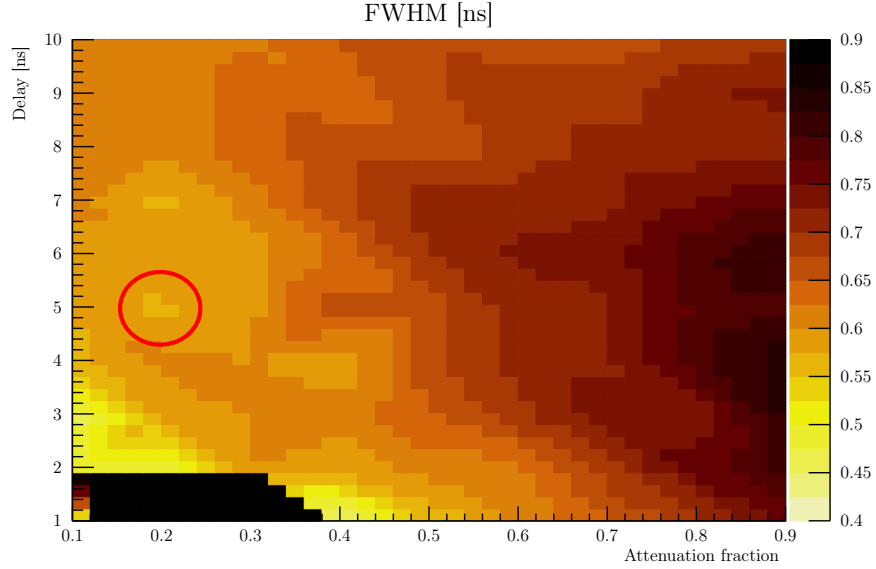


Figure 14: FWHM of the time differences distribution as function of CFTD parameters. The chosen minimum is in the red circle.

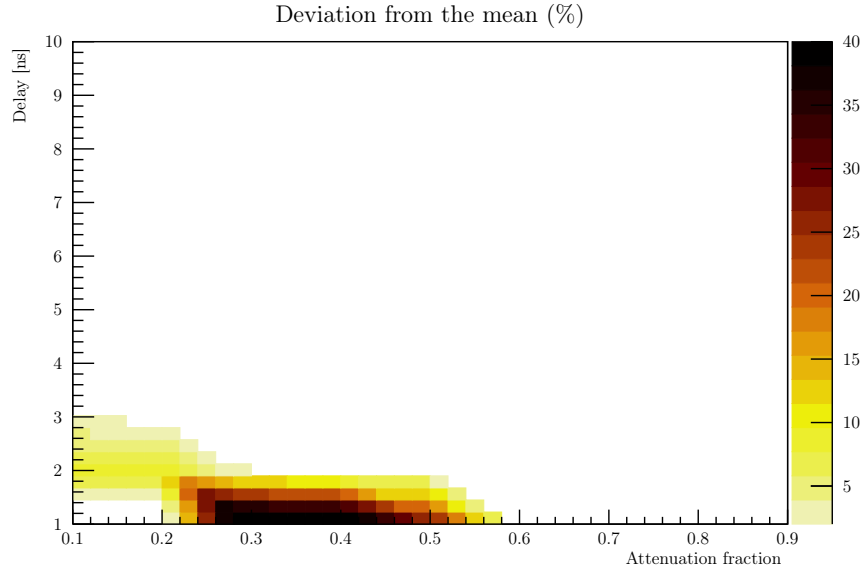


Figure 15: Deviations of the position of the TAC peak computed for each parameter configuration from the mean.

Note that in fig 14 data in the low- τ low- f region must be discarded, as in that area the means of the TAC peaks are strongly incompatible with the others configurations (fig 15). This is probably due to problems in finding the zero-crossing point. The best choice for the attenuation fraction and the delay is then the same of the analog CFTD: $f \sim 0.2$ and $\tau \sim 5$ ns.

From the theory the best choice for the delay given the fraction is $\tau = (1 - f)t_{rise}$ where t_{rise} is the rise time of the signals (in our case, $t_{rise} \sim 6$ ns): this trend is roughly visible in fig 14.

8.4 Time resolution and energy threshold

Keeping the best settings for fraction and delay, the FWHM of the TAC peak has been computed as function of the energy threshold, as done for the analog CFTD in sect. 6.

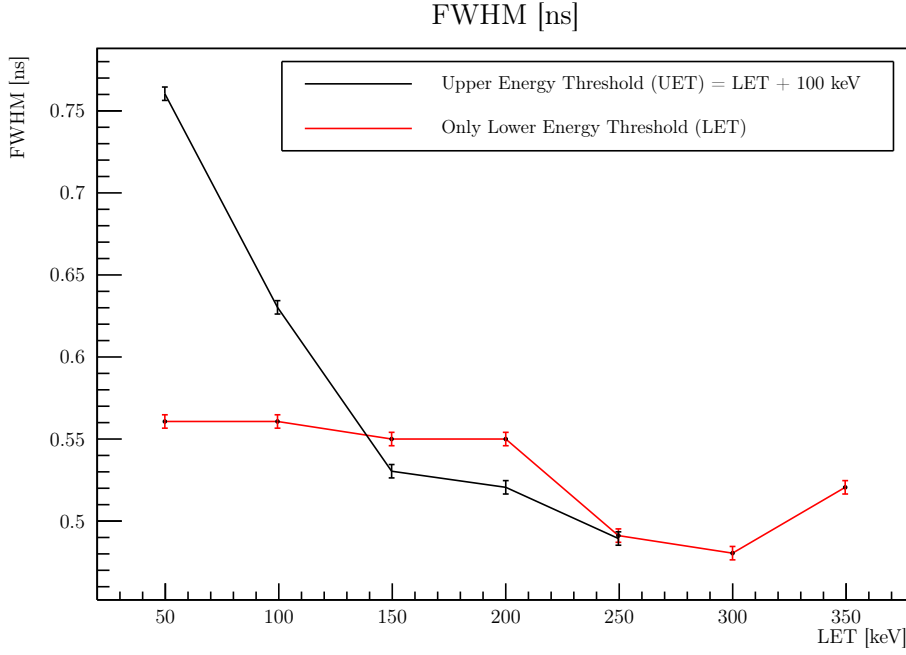


Figure 16: FWHM of the TAC peak as a function of energy threshold.

As can be seen from fig 16 results are very similar to the analog version, and in both cases best resolution is achieved considering the events whose energy is around the Compton edge ($\sim 300\text{keV}$ for ^{22}Na).

The best resolution achieved by the a-posteriori CFTD is $\sim 0.5\text{ns}$ while the best one achieved by the analog one is $\sim 0.3\text{ns}$. The main reason for this can be found in the fact that the digital waveforms are sampled each 1ns , a coarse sampling ratio considering the resolutions we're working with.

9 Conclusions

With respect to the initial aims:

- The energy spectra have been successfully calibrated through the Compton edge and the half maximum position;
- The external delay has been optimized to enhance peak resolution; the optimal delay has been found around 5ns , as theoretically expected;
- The best time resolution has been achieved filtering in energy around the Compton edge;
- The speed of light has been measured, obtaining a value compatible with the real one;
- A comparison between analog CFTD and a simulated a-posteriori one has been done, finding that they provide similar resolution, even if the analog one is slightly better.